Numerical Simulation Studies of Gas Production Scenarios From Hydrate Accumulations at the Mallik Site, Mackenzie Delta, Canada

George J. Moridis [(1)]*, Timothy S. Collett [(2)], Scott R. Dallimore [(3)]
Tohru Satoh [(4)], Stephen Hancock [(5)] and Brian Weatherill [(5)]

[(1)] Lawrence Berkeley National Laboratory, University of California, Berkeley, California 94720, USA;
[(2)] United States Geological Survey, Denver, Colorado 80225-0046, USA;
[(3)] Geological Survey of Canada, Sidney, British Columbia V8L 4B2, Canada;
[(4)] Japan National Oil Corporation, Chiba 261-0025, Japan;
[(5)] Adams Pearson Associates Inc., Calgary, Alberta T2P 3T6, Canada

The Mallik site represents an onshore permafrost-associated gas hydrate accumulation in the Mackenzie Delta, Northwest Territories, Canada. An 1150 m deep gas hydrate research well was drilled at the site in 1998. The objective of this study is the analysis of various gas production scenarios from several gas-hydrate-bearing zones at the Mallik site. The TOUGH2 general-purpose simulator with the EOSHYDR2 module were used for the analysis. EOSHYDR2 is designed to model the non-isothermal CH_4 (methane) release, phase behavior and flow under conditions typical of methane-hydrate deposits by solving the coupled equations of mass and heat balance, and can describe any combination of gas hydrate dissociation mechanisms. Numerical simulations indicated that significant gas hydrate production at the Mallik site was possible by drawing down the pressure on a thin free-gas zone at the base of the hydrate stability field. Gas hydrate zones with underlying aquifers yielded significant gas production entirely from dissociated gas hydrate, but large amounts of produced water. Lithologically isolated gas-hydrate-bearing reservoirs with no underlying free gas or water zones, and gas-hydrate saturations of at least 50% were also studied. In these cases, it was assumed that thermal stimulation by circulating hot water in the well was the method used to induce dissociation. Sensitivity studies indicated that the methane release from the hydrate accumulations increases with gas-hydrate saturation, the initial formation temperature, the temperature of the circulating water in the well, and the formation thermal conductivity. Methane production appears to be less sensitive to the rock and hydrate specific heat and permeability of the formation.

1 Introduction

1.1 Background. The Mallik site represents an onshore permafrost-associated methane hydrate accumulation in the Mackenzie Delta, Northwest Territories, Canada. An 1150 m deep gas hydrate research well was drilled at the site in 1998, and led to the first significant body of field data from an Arctic natural gas hydrate deposit (Dallimore et al., 1999). In this paper we analyze various gas production scenarios for several gas-hydrate-bearing stratigraphic zones at the Mallik site.

1.2 The Numerical Code. The analysis of the production scenarios in this paper were conducted using the TOUGH2 general-purpose simulator (Pruess et al., 1999) for multi-component, multiphase fluid and heat flow and transport in the subsurface with the EOSHYDR2 module (Moridis et al., 1998; 2002). EOSHYDR2 can model the non-isothermal methane release, phase behavior and flow under conditions typical of methane-hydrate deposits (i.e., in the permafrost and in deep ocean sediments) by solving the coupled equations of mass and heat balance.

EOSHYDR2 includes both equilibrium and a kinetic model of gas hydrate formation and dissociation. The model accounts for up to nine components (hydrate, water, native methane and methane from hydrate dissociation, a second native and dissociated hydrocarbon, salt, water-soluble inhibitors and a heat pseudo-component). The mass components are distributed among four phases, i.e., a gas phase, a liquid phase, and two solid immobile phases: an ice phase and the hydrate phase. The thermophysical properties of the various mass components can be described at temperatures as low as –110 °C. Dissociation, phase changes and the corresponding thermal effects are fully described, as are the effects of salt and hydrate inhibitors. The model can describe gas hydrate dissociation involving any combination of the possible dissociation mechanisms (i.e., depressurization, thermal stimulation, and salting-out effects).

2 Simulation Zones

A total of five zones were investigated. In all the zones the porosity (ϕ = 0.28), the intrinsic permeability (k = 20 mD), the thermal conductivity (k_θ = 1.5 W/m °C), the rock specific heat (C_R = 800 J/kg °C), and the hydrate specific heat (C_H = 1600 J/kg °C) were assumed to be the same. The regional plunge along the crest of the Mallik structure was not considered in the simulations because of the very shallow dip angle (2 degrees to the northwest) and the limited extent of the affected hydrate accumulations during the dissociation process. In all simulations, (a) a gas hydrate equilibrium process was

* Corresponding author. E-mail: gjmoridis@lbl.gov

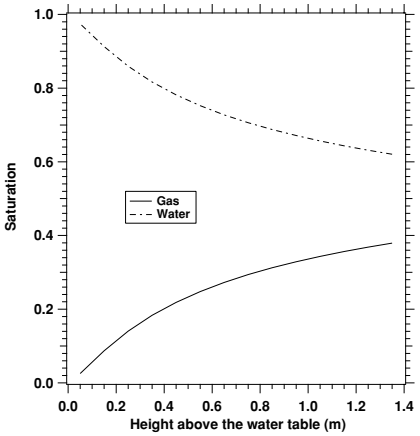

Fig. 1. Water and gas saturation in the two-phase layer in Zone #1.

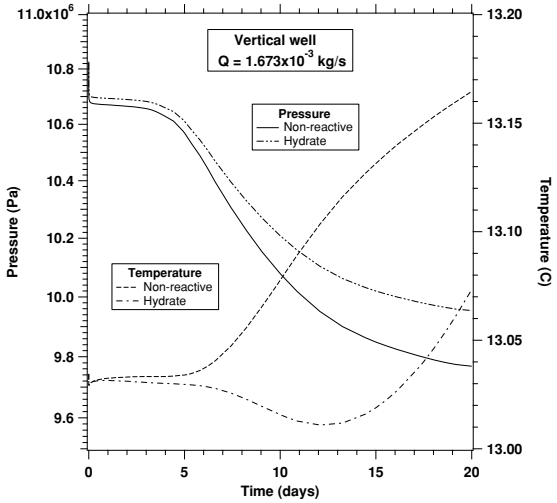

Fig. 2. Evolution of pressure and temperature at the well in Zone #1.

assumed, (b) a heat flux corresponding to the geothermal gradient of 0.03 ºC/m was applied to the bottom of the simulated domain, and (c) the gas hydrate was assumed to be a simple methane-hydrate (thus, the native gas, where present, was 100% methane). Relative permeabilities were obtained from the Corey (1954) model, and capillary pressures were computed from the Parker et al. (1987) model. In both cases, the irreducible aqueous and gas saturations in all zones were assumed to be 0.2 and 0.05, respectively.

2.1 Zone #1. Zone #1 is characterized by a 20-m-thick hydrate accumulation, the base of which (at a depth of 1100 m) marks the bottom of the hydrate stability zone. The temperature at the bottom of the hydrate layer is T = 13ºC, i.e., the gas hydrate equilibrium temperature at the formation pressure of P = 10.8 MPa. The gas hydrate interval has a hydrate saturation S_H=0.8, the rest being water. In the simulation this interval is capped by a water-saturated siltstone/mudstone sequence that acts as a flow boundary, and is underlain by a thin (1.4-m-thick) layer in which gas and liquid water (a brine) coexist. The water and gas saturations in the two-phase zone are shown in Figure 1. It was assumed, that the two-phase zone is underlain by a 15-m-thick water-saturated sandstone unit bounded at the bottom by a tight (no-flow) unit. Zone #1 and its boundaries extend uniformly over a large area. Since this zone is in immediate contact with the gas hydrate stability zone, relatively small pressure and/or temperature changes can cause gas hydrate dissociation. Additionally, the presence of the thin two-phase (gas and brine) layer allows the depressurization of the overlying gas hydrates, which in turn can induce gas production through gas hydrate dissociation.

In this study we considered only depressurization of the hydrate interval through a single vertical well completed in the two-phase layer. The cylindrical 2-D semi-infinite reservoir model in this set of simulations was discretized into 56 and 64 non-uniform gridblocks in r and z, respectively, for a total of 3584 gridblocks. Five components (hydrate, water, native methane, methane originating from gas hydrate dissociation, and salt) and heat were accounted for, resulting in system of 21504 simultaneous equations. To obtain an accurate estimate of the contribution of dissociated gas to the total gas production, the native methane was considered separately from the hydrate-released methane (hereafter referred to as 'dissociated methane'). Fluids were produced from the well at a cumulative rate of Q = $1.67\text{x}10^{-3}$ kg/s, determined through trial-and-error to allow gas production without water flooding for a period of at least 30 days.

Brine and gas (mostly methane with minor water vapor) were distributed in the production stream according to their mobilities in the vicinity of the well. To quantify the effects of the dissociating gas hydrates, two sets of simulations were conducted. In the first set, the gas hydrate layer was assumed to be inert (i.e., non-dissociating), while hydrate dissociation was accounted for in the second set. This approach was implemented to determine whether the two systems had a markedly different response.

The evolution of pressure and temperature at the well (averaged over the completion interval) for the two simulation sets are shown in Figure 2. Simulations suggest the pressure in Zone 1 is significantly higher when gas hydrate dissociation is considered. This is consistent with expectations because of the contribution of the dissociated methane to the total pressure. The differences in the temperature response are interesting. For non-dissociating gas hydrates, the temperature rises very slowly (practically imperceptibly) initially, and is then followed by a rapid temperature increase as warmer water from deeper in the aquifer is drawn to the well. For dissociating gas hydrates, a temperature drop is first observed. This is expected because of the strongly endothermic nature of gas hydrate dissociation. However, the temperature begins to increase after the initial drop as deeper warmer water moves to the well.

Figure 3 shows the mass fraction of gas in the production stream. By maintaining a low total mass production rate, the gas mass fraction is practically one for about 6 days, at which time it begins to decline. Note that maintaining high gas production is challenging in Zone #1 because of (a) the limited thickness of the two-phase zone, (b) the proximity to the underlying infinite aquifer, and (c) the

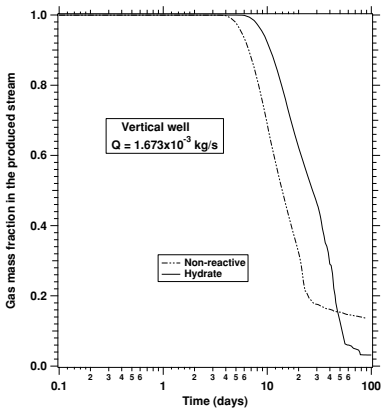

Fig. 3. Gas mass fraction in the production stream of the well in Zone #1.

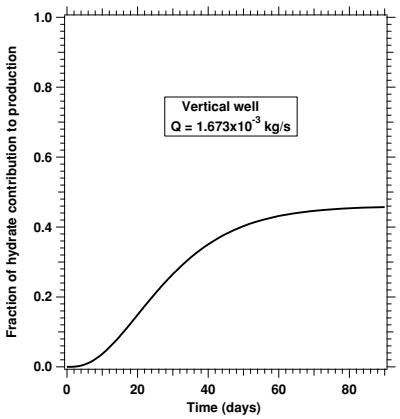

Fig. 4. Hydrate contribution to gas production stream in Zone #1.

large amounts of water released in the course of gas hydrate dissociation. The contribution of dissociated methane to the production stream (Figure 4) shows that it rises from zero to about 0.46 in about 60 days, after which time it remains constant. This indicates that gas-hydrate dissociation is a significant source of gas, contributing about half of the produced gas in this geologic scenario.

2.2 Zone #2. Zone #2 is characterized by a 16-m-thick hydrate-bearing interval (from 899 to 915 m, with T = 7.5 °C, P = 9 MPa, and S_H=0.5) capped by a relatively thick gas-hydrate-bearing sandstone sequence with varying gas-hydrate saturations. This gas hydrate accumulation is underlain by a 2-m-thick water-saturated layer, followed by a 2-m-thick low-porosity (ϕ<2%) sandstone that is assumed to act as a flow boundary. Because of its shallower depth, Zone #2 is cooler than Zone #1. Zone #2 and its boundaries are assumed to extend uniformly over a large area.

As in Zone #1, the only dissociation method we considered was depressurization of the gas hydrate accumulation through fluid withdrawals from the underlying water-saturated zone.

The cylindrical 2-D grid involved 65 and 38 non-uniform gridblocks in r and z, respectively, for a total of 2210 gridblocks. The simulations accounted for heat and four components (hydrate, water, dissociated methane, and salt), resulting in a system of 12350 simultaneous equations.

Water was produced from the well (completed in the 2-m water-saturated layer) at a rate of Q_w = 0.58 kg/s (a rate than can be sustained without cavitation). The rate of the corresponding methane production was computed internally by the numerical model from the aqueous and gas phase mobilities near the wellbore.

Figure 5 shows the cumulative gas production over time. Note that the gas phase emerges only after about 5 days of continuous water production. There are two reasons for the delay in gas appearance. The first is the adverse relative permeability conditions (emergence of a gas phase in a previously fully-saturated formation, coupled with the release of large amounts of water during dissociation) that necessitate a gas saturation $S_g > 0.05$ for gas mobility. The second reason is the low initial temperature (at the formation pressure of 9 MPa, the dissociation temperature is 11.5 °C) that requires a larger pressure drop (and, thus, longer fluid withdrawal) to effect dissociation through depressurization. Note that the cumulative gas production tends to a plateau as pressure approaches a steady-state distribution (with the boundaries replenishing the withdrawn water) and the gas hydrate reach a new pressure-temperature equilibrium point.

An important observation from Figure 5 is that a large volume of gas can be produced from Zone #2, and all of it is attributable to gas hydrate dissociation. While this is promising, the potential of this single-well approach is limited by the large volume of produced water. This is demonstrated by the very low gas mass fraction in the production stream (Figure 6), which does not exceed 0.017 over the simulation period.

2.3 Zones #3, #4 and #5. These three zones are discussed together because they are all characterized by the absence of any layers of mobile gas or water. In these zones, the pore space is occupied primarily by gas hydrate and water (mostly immobile water).

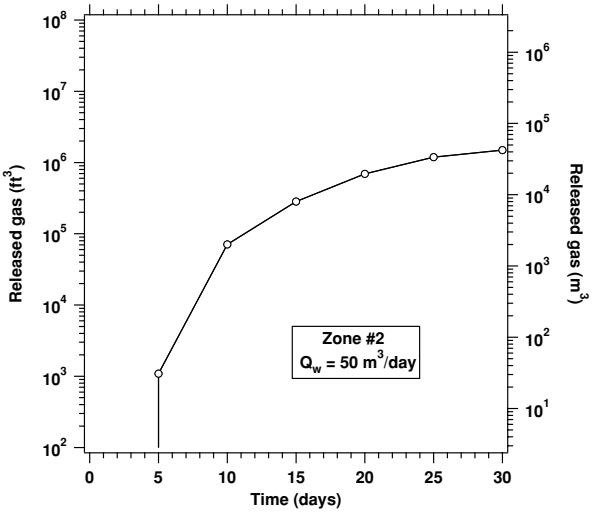

Fig. 5. Cumulative gas production in Zone #2.

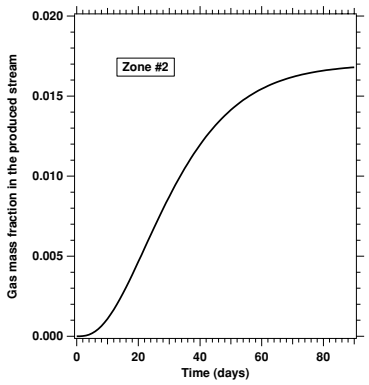

Fig. 6. Gas mass fraction in the production stream of Zone #2.

In Zone #3 (T = 12.8 °C, P = 10.74 MPa, and S_H = 0.8) the gas hydrate interval extends from a depth of about 1081 m to 1091 m. It is capped by a relatively thick siltstone sequence, and is underlain by a relatively thick gas-hydrate-bearing sandstone sequence with varying gas-hydrate saturations. Zone #4 (T = 10.5 °C, P = 10.0MPa, and S_H = 0.5) extends from a depth of 1007 m to 1017 m, and is capped and underlain by relatively thick sandstone sequences with varying gas-hydrate saturations. Zone #5 (P = 8.9 MPa, and S_H = 0.8) is shallower (905 m to 915 m) and colder (T = 7.5 °C), and its top and bottom boundaries are similar to those of Zone #4.

Because of the high S_H in all three zones, the relative permeability to both the aqueous and the gas phases are assumed to be very small. This would suggest that flow is severely restricted, and that pressure changes are expected to penetrate a limited portion of the gas-hydrate-bearing reservoir. Because of the adverse permeability conditions, we evaluated thermal stimulation only for gas hydrate dissociation in Zones #3 through #5. The production strategy we investigated involved the circulation of hot water in a single vertical well completed in the gas hydrate interval.

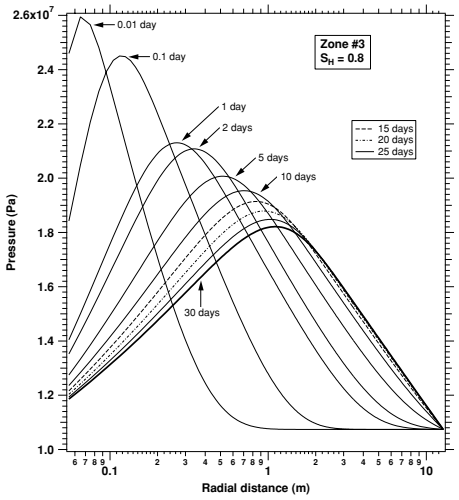

Fig. 7. Formation pressure during thermal dissociation of hydrates in Zone #3.

The same cylindrical 2-D grid was used in the simulations of gas hydrate dissociation in Zones #3, #4 and #5. The hydrate zones were separated into 82 and 20 non-uniform gridblocks in r and z, respectively, for a total of 1640 gridblocks. The simulations accounted for heat and three components (hydrate, water, and dissociated methane), resulting in a system of 6560 equations. In all simulations, the wellbore temperature was maintained at 50 °C, and the well was kept at the corresponding hydrostatic pressure.

Figure 7 shows the evolution of pressure (averaged over the gas hydrate interval) as Zone #3 is exposed to the hot water. The observed pressure surge exceeds the hydrostatic fluid pressure by a factor of as high as 2.5. The reason for the very high pressure is the sudden release of the large volume of methane from the dissociating gas hydrate (1 m^3 of hydrate releases 164 m^3 of methane under standard conditions) in response to the thermal stimulation. This is a more effective mechanism than depressurization, as the gas hydrate equilibrium pressure-temperature relationship indicates (Moridis, 2002). The large methane volume is released into the limited pore space that was previously occupied by only the nearly incompressible water. This, coupled with the extremely low effective permeability of the gas-hydrate-bearing formation (a result of S_H = 0.8), which does not allow the gas to move radially away from the well and the pressure to dissipate, causes the pressure spike. The peak pressure decreases over time as the dissociation front advances (and thus the corresponding permeable pore space increases).

Figure 8 shows the distribution of temperature over time during the same period. Note the absence of a discernible temperature drop at the leading edge of the advancing temperature front. This indicates that the system thermal conductivity (probably the grain-to-grain contact of the more conductive solid grains) is sufficiently large to provide the needed dissociation heat. Another important observation from Figure 8 is that the reach of the temperature front during the 30-day simulation period is only about 4 m. This is indicative of the position of the dissociation front, although of limited accuracy because of the shifting dissociation temperature

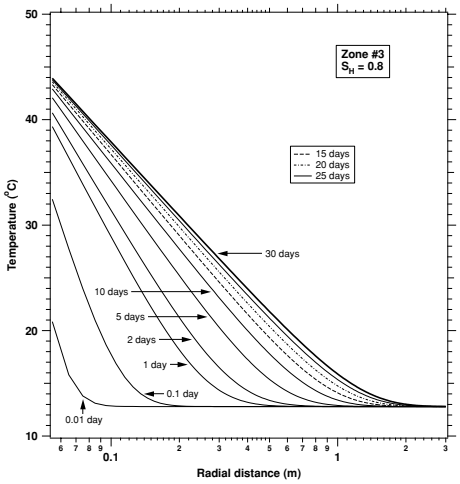

Fig. 8. Temperature distribution during thermal dissociation of hydrates in Zone #3.

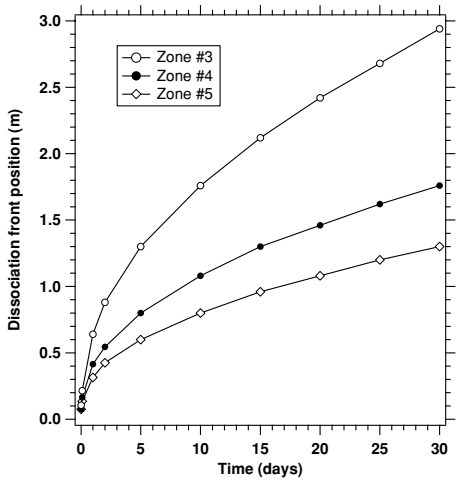

Fig. 9. Radii of the dissociation fronts in Zones #3 to #5.

(because of the increase in pressure – Figure 7). The position of the dissociation fronts in Zones #3, #4 and #5 over time is shown in Figure 9. In Zone #3, the dissociation front at t = 30 days is at a radius of only about 3 m, confirming the indications of the temperature profile. The dissociation radius is significantly smaller in Zone #4, and even smaller in the much colder Zone #5.

The cumulative gas production in Zones #3, #4 and #5 is shown in Figure 10. The volume of the dissociated gas from Zone #3 is about 5 times larger than the corresponding volumes from Zone #5. This significant difference is due to the higher temperature that is close to the dissociation temperature at the pressure of Zone #3. Thus, heat addition is used mostly for dissociation, without being consumed to raise the temperature of the hydrate (a relative insulator). This is demonstrated by the gas production from the much colder Zone #5, which is smaller by a factor of five than that from Zone #3 despite having the same S_H = 0.8. Although the dissociation front advances much further in Zone #4 (Figure 9), the volume of the released gas is about the same as that from Zone #5 because of the lower S_H = 0.5.

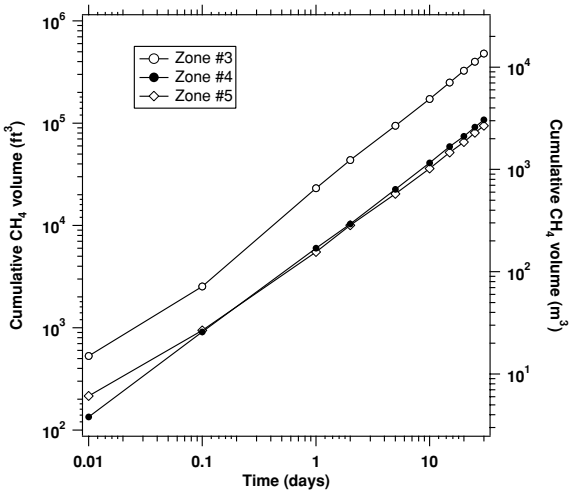

Fig. 10. Cumulative gas production in Zones #3, #4 and #5 (volumes in standard conditions).

3 Sensitivity Analysis

Sensitivity analyses were conducted for production from thermal dissociation to assess the importance of gas hydrate saturation, formation temperatures and thermal conductivity under uniform conditions. The importance of gas-hydrate-saturation is shown for Zone #4 in Figure 11, which shows a substantial (but sublinear) increase in the volume of the released gas when S_H increases from 0.5 to 0.8. Figure 12 compiles the effect of formation temperature and thermal conductivity on gas release versus time using the gas production form Zone #5 as a baseline. The effect of the thermal conductivity (varied from the baseline value of 1.5 W/m/°C) on gas production appears to be linear. The initial T appears to have a dramatic effect on gas production. Thus, a 3.5 °C temperature difference (between T in Zone #5 and the hydration T_H of 11 °C at the formation pressure), is shown to reduce production by a factor of about four. This behavior is due to the substantial amount of heat needed to raise the temperature of the hydrate (a relative thermal insulator) to the dissociation temperature. When the well temperature T_w increases from 50 °C to 70 °C, the produced gas volume increases only mildly (i.e., by about 30%). The reason for this modest increase is the heat flux into the hydrate interval decreasing rapidly over time as the temperature differential decreases, and the higher well temperature is insufficient to counteract the temperature differential decline.

The pressure conditions at the well combined with the manner of heat addition appear to have the most dramatic effect on gas production. Thus, heat addition at a constant rate of 6 kW increases gas production by 40% when the wellbore is kept at the hydrostatic pressure of the circulating water (denote by *a* in Figure 12). When, however, heat is added at the same rate and the well is kept dry at atmospheric pressure (for example by artificial lift production of all water released during dissociation), then gas production increases by about an order of magnitude (denoted by *b* in Figure 12). This is due to the combined effect of thermal stimulation of the gas hydrate and depressurization (as the hydrate interval is exposed to atmospheric rather than hydrostatic pressure).

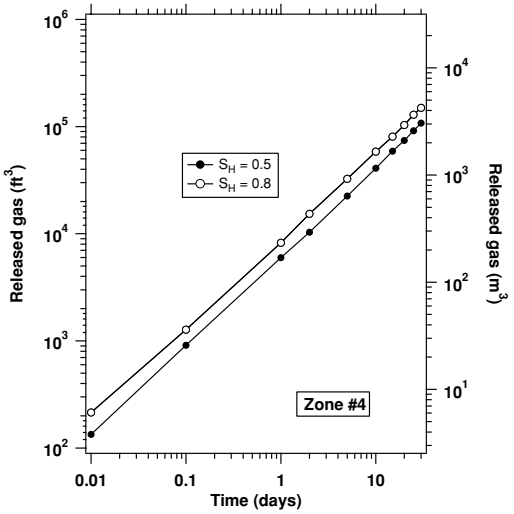

Fig. 11. Sensitivity of gas production to S_H in Zone #4.

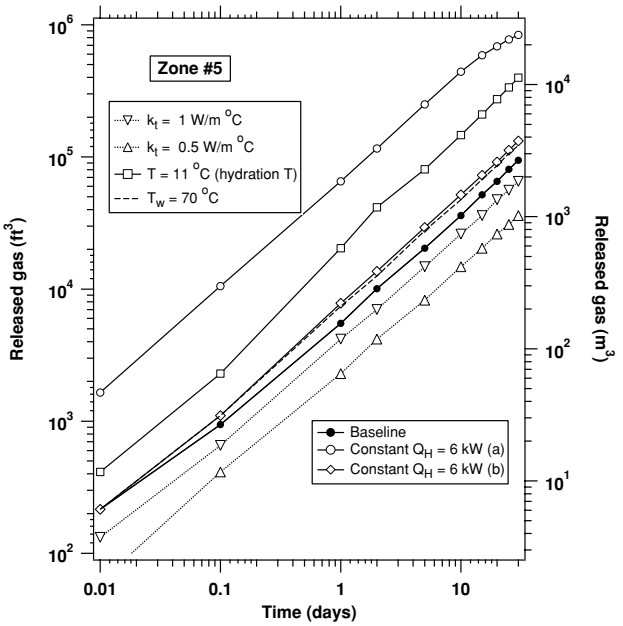

Fig. 12. Sensitivity of gas production to thermal conductivity k_t, hydrate temperature T, method of heat addition, and well boundary conditions.

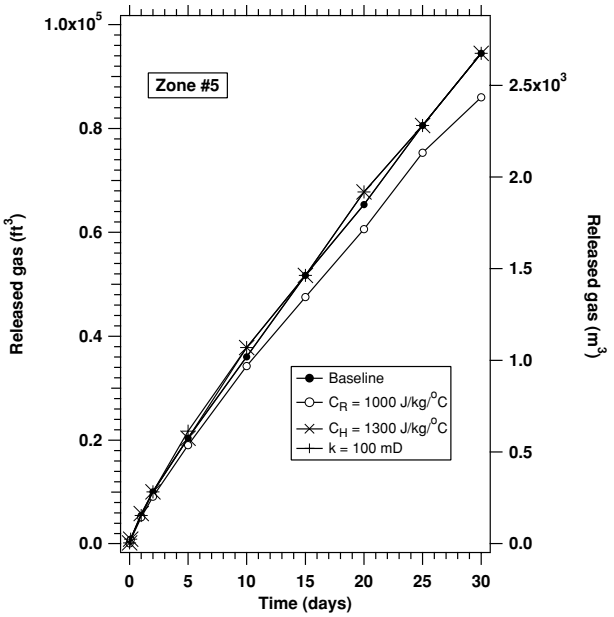

Fig. 13. Sensitivity of gas production to hydraulic conductivity k, rock specific heat C_R and hydrate specific heat C_H.

Conversely, gas production under the aforementioned conditions appears to be practically insensitive to the formation permeability k (because of the very high pressures and the limited dissociation zone) and to the specific heat C_H of the gas hydrate (because the hydrate is not the dominant component in the system). Gas production is very mildly affected by the specific heat C_R of the rock (Figure 13).

4 Conclusions

The following conclusions can be drawn from the numerical simulation study of gas production from five zones at the Mallik site:

1. Production from Zone #1 (with a free gas zone underlying the gas hydrate deposit) by depressurization is possible.

2. Depressurization of Zone #2 (a gas hydrate underlain by an aquifer) yields gas but also large amounts of water.

3. In Zones #3 through #5 (gas hydrates with no underlying free-gas or water zones, and a gas-hydrate saturation of at least 50%) thermal stimulation yields measurable amounts of dissociated gas.

4. Under the conditions of Zones #3 through #5, sensitivity studies indicate that the gas production from the hydrate accumulations increases with the gas-hydrate saturation, the hydrate initial temperature, the temperature of the circulating water in the well, and the thermal conductivity of the system. Gas production appears to be less sensitive to the rock and gas hydrate specific heat and the permeability of the formation.

Acknowledgments

This work was supported by the Assistant Secretary for Fossil Energy, Office of Natural Gas and Petroleum Technology, through the National Energy Technology Laboratory, under U.S. Dept. of Energy Contract No. DE-AC03-76SF00098. The authors are indebted to Stefan Finsterle and John Apps for their insightful review comments.

References

Corey, A.T. (1954). The interrelation between gas and oil relative permeabilities. *Producers Monthly*, 38-41.

Dallimore, S.R., Uchida, T., & Collett, T.S. (1999), eds.. Scientific Results from JAPEX/JNOC/GSC Mallik 2L-38 Gas Hydrate Research Well, Mackenzie Delta, Northwest Territories, Canada, *Geological Survey of Canada Bulletin* **544**.

Moridis, G.J., Apps, J., Prues, K., & Myer, L. (1998). EOSHYDR: A TOUGH2 module for CH4-hydrate release and flow in the subsurface. *Report LBNL-42386*, Lawrence Berkeley National Laboratory, Berkeley, CA.

Moridis, G.J. (2002). Numerical simulation of gas production from methane hydrates. *SPE 75691*, To appear in the Proceedings, SPE 2002 Gas Technology Symposium, Calgary, Alberta, Canada, April 30-May 2, 2002.

Parker, J.C., Lenhard, R.J., & Kuppusamy, T. (1987). A parametric model for constitutive properties governing multiphase flow in porous media. *Water Resour. Res.* **23**(4), 618-624.

Pruess, K., Oldenburg, C., & Moridis, G. (1999). TOUGH2 User's Guide – Version 2.0. *Report LBL-43134*, Lawrence Berkeley national Laboratory, Berkeley, CA.